Wang, Dong; Yang, Haiying; Wang, Qingxiang; Lu, Yi; Yan, Jie; Cheng, Wanli; Rojas, Orlando J.; Han, Guangping

# Composite membranes of polyacrylonitrile cross-linked with cellulose nanocrystals for emulsion separation and regeneration

*Published in:*
Composites Part A: Applied Science and Manufacturing

*DOI:*
10.1016/j.compositesa.2022.107300

Published: 01/01/2023

*Document Version*
Publisher's PDF, also known as Version of record

Composites: Part A 164 (2023) 107300

Contents lists available at ScienceDirect

Composites Part A

journal homepage: www.elsevier.com/locate/compositesa

# Composite membranes of polyacrylonitrile cross-linked with cellulose nanocrystals for emulsion separation and regeneration

Dong Wang [a,b,1], Haiying Yang [a,1], Qingxiang Wang [a], Yi Lu [b], Jie Yan [a], Wanli Cheng [a,*], Orlando J. Rojas [b,c,*], Guangping Han [a,*]

[a] Key Laboratory of Bio-based Material Science and Technology (Ministry of Education), Northeast Forestry University, 26 Hexing Road, Harbin 150040, China
[b] Bioproducts Institute, Department of Chemical & Biological Engineering, Department of Chemistry, and Department of Wood Science, The University of British Columbia, Vancouver, British Columbia V6T 1Z3, Canada
[c] Department of Bioproducts and Biosystems, School of Chemical Engineering, Aalto University, Vuorimiehentie 1, Espoo FI-00076, Finland

ARTICLE INFO

*Keywords:*
A. Cellulose
A. Nanocomposites
A. Polymer-matrix composites (PMCs)
E. Electrospinning

ABSTRACT

As a result of fatigue and damage, the durability of separation membranes remains a major challenge for long-term use in the separation of multiphase systems, such as oily water and emulsions. Here, we synthesize electrospun membranes based on hydrolyzed polyacrylonitrile reinforced with cellulose nanocrystals (CNC). The nanofibers form highly porous systems that are held together by crosslinking, allowing fast mass transport while achieving high tensile strength and elongation at break. The membranes exhibit shape retention upon immersion in complex fluids. An underwater oil contact angle of 141° enables efficient emulsion separation (98.2 % separation at a flux as high as 1293 $L \cdot m^{-2} \cdot h^{-1}$ for hexane-in-water emulsions) and reliable operation for at least 20 filtration cycles. A similar performance is achieved in the separation of emulsions based on toluene, petroleum ether, diesel, and vegetable oils. Overall, the designed composite membranes endow stable three-dimensional structures, excellent durability, and separation performance.

## 1. Introduction

Industrial oily wastewater and oil spills have become an increasingly serious environmental and ecosystem challenge [1–5]. Gravity separation, distillation, air flotation, electrophoresis, flocculation, centrifugation, and absorption are some of the approaches adopted for oil–water separation [6–10]. However, these methods suffer from complex manufacturing processes, relatively high costs, low separation efficiency, and high energy consumption. These factors have greatly limited practical implementation [11–14]. Hence, there is a growing demand for new routes to separate oil–water mixtures, especially considering high-efficiency membrane-based separation of low energy consumption and cost [15–17].

The approaches used to synthesize membranes determine their intrinsic properties [18]. Therein, electrospinning has been considered due to its simplicity, and high efficiency in producing nano-scaled fibers [19–22]. These nano-fibers can be assembled into ordered arrays or hierarchical structures by manipulating the spinning procedures [23]. Moreover, such electrospun nanofibrous membranes (ENMs) feature special advantages, such as high surface area-to-volume ratios, interconnected pore structures, and well-controlled composition [24,25], making them a preferred choice for low-resistance liquid filtration media.

One of the most crucial factors for efficient oil–water separation is the design of selective wettability [26–28]. In this respect, PAN nanofibers have selectivity for water and oil and are suitable for filtration operations underwater. In addition, PAN has superior thermal, and chemical stability [29]. Unfortunately, PAN nanofibers have poor mechanical strength since they stack on each other with weak inter-fibers adhesion [30]. To address this issue, cellulose nanocrystals (CNC) can be considered as a reinforcement phase while we note that CNC is not soluble neither in common organic solvents or water- [31]. CNC molecular chain contains abundant hydroxyl groups, which can form intramolecular or intermolecular hydrogen bond interactions, thereby enhancing the mechanical strength and structural stability of the nanofiber membranes [32]. In addition, CNC has excellent chemical resistance [33].

Previous studies have shown that hydrolysis leads to changes in the

* Corresponding authors.
*E-mail addresses:* nefucwl@nefu.edu.cn (W. Cheng), orlando.rojas@ubc.ca (O.J. Rojas), guangping.han@nefu.edu.cn (G. Han).
[1] Authors contributed equally.

https://doi.org/10.1016/j.compositesa.2022.107300
Received 29 August 2022; Received in revised form 19 October 2022; Accepted 1 November 2022
Available online 5 November 2022

surface of PAN [34], while the inner structure remains unaffected, which is an advantage to maximize the strength. Hence, hydrolysis has been applied on the surface of PAN-based ENM to activate the nitrile group (—CN) by surface conversion to carboxyl groups (—COOH), effectively enhancing the underwater oil repellency and antifouling performance [35].

Although oil–water separation has been a critical topic of discussion, there is still only a limited understanding of the properties that are necessary for the application of membranes. Here, we hypothesize that the introduction of the hydrogen-bonding with CNC has the potential to lead to ENMs with excellent structural stability. Therefore, hydrophilic CNC was combined with PAN to produce nanofiber membranes via electrospinning. The CNC/PAN composite nanofiber membranes were then hydrolyzed with NaOH solution (Fig. 1), yielding CNC/H-PAN systems. The CNCs formed cross-linking networks *via* hydrogen bonding with the carboxyl groups of H-PAN. The effect of CNC on the micro-morphology and mechanical strength of the membranes was investigated before and after modification. The properties of CNC/H-PAN nanofibers, especially the surface functional groups, pore size distribution, wettability, separation flux, and separation efficiency, were analyzed to elucidate the property-structure relationships and oil–water separation efficiency. Our results indicated that cellulose nanocrystals strengthened the membranes and preserved the integrity of their three-dimensional structure when immersed in aqueous media. Meanwhile, the hydrolysis process endowed hydrophilicity. Overall, we prepare high-performance nanofiber membranes with excellent performance in the separation of oil/water emulsions [36,37].

## 2. Experiments

### 2.1. Materials

Cellulose nanocrystals were prepared by acid hydrolysis [38]. PAN (Mw = 85 000) was purchased from Dibo Biotechnology (Shanghai, China). Sodium dodecyl sulfate (SDS) and oil red (Sudan III) were provided by Aladdin (Shanghai, China). N, *N*-Dimethylacetamide (DMAc), dimethylformamide (DMF), sodium hydroxide (NaOH), petroleum, toluene, and *n*-hexane, and were obtained from Kermel (Tianjin, China). Diesel oil was obtained from Sinopec Group (Harbin, China) and soybean oil was obtained from a local supermarket (Harbin, China).

### 2.2. Fabrication of the nanofibrous membranes (ENMs)

First, CNC (0–20 wt%) was suspended in DMF (20 g) under ultrasonication (100 W, 3 min) in an ice water bath. Then, PAN (3.2 g) was dissolved in the CNC suspension and stirred at 50 °C to obtain a homogeneous CNC-*x*/PAN spinning solution, where × is the CNC-to-PAN ratio (mass basis).

An electrospinning system (SS-2535H, Yong Kang Le Ye, China) was used to prepare the ENMs. The spinning precursor was added to a 10 ml syringe connected to a 19-G needle (1.12 mm inner diameter). The positive and negative voltage between the needle and the roller collector was + 15.0 kV and −3.0 kV, respectively. The spinning rate, spinning distance, and rotational speed of the collector were 0.06 mm/min, 22 cm, and 80 rpm, respectively. All experiments were carried out at room temperature, and relative humidity of 25 ± 5 %. After electrospinning, the ENMs were subjected to surface hydrolysis. For this purpose, the ENMs (5 cm × 5 cm) were immersed in 4 wt% NaOH solution at 60 °C for 45 min, then removed and rinsed in deionized water. Next, the ENMs were immersed in 4 wt% HCl solution for 30 min, then rinsed until the pH of the solution was 7. Finally, the modified ENMs were dried in a vacuum oven at 60 °C for 24 h. The conversion of carboxyl groups in the membranes was 10.2 % (Supporting Information).

### 2.3. Characterization

The morphology of the nanofibers was analyzed by scanning electron microscopy (SEM, JSM-7500F, Japan). The diameter of the nanofibrous membrane was measured from the SEM images by Nano Measurer software. The mechanical properties of the CNC/H-PAN membranes were analyzed with a mechanical testing unit (WDW-20, Chengde Mechanical Instrument Co., Ltd, China). The size of the samples was

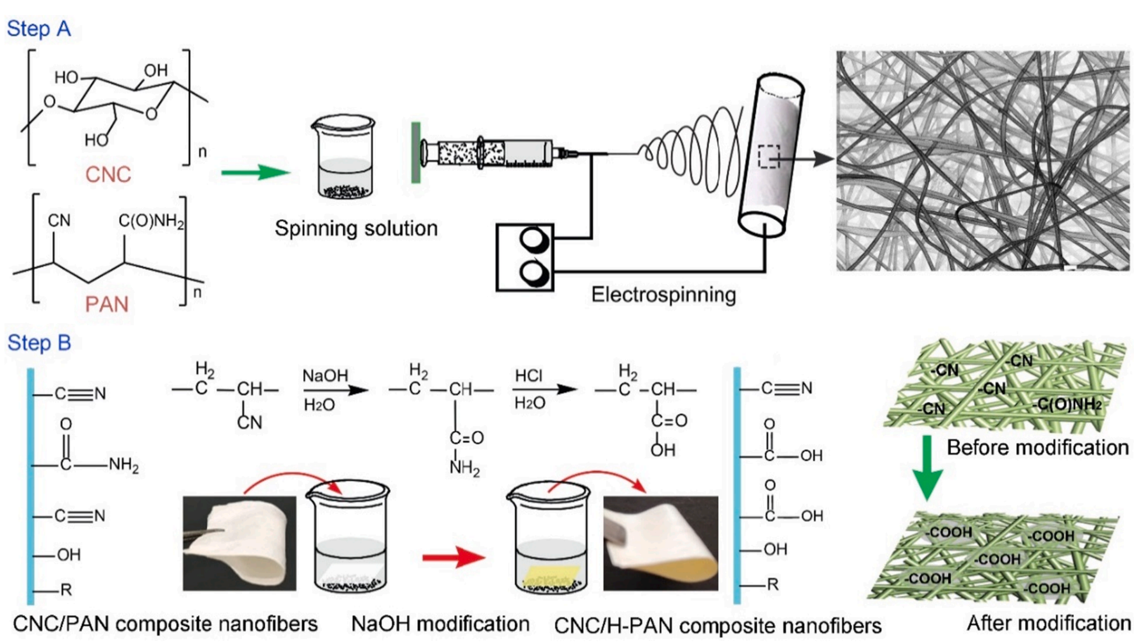


**Fig. 1.** Preparation process of the CNC/H-PAN nanofibrous membranes. (Step A) Electrospinning process: Nanofibrous membranes were prepared by electrospinning of a colloidal suspension of CNC and PAN. (Step B) CNC/H-PAN membranes were synthesized *via* partial hydrolysis of PAN, following three major steps: $OH^-$ initiates a nucleophilic attack on the carbon atoms on the —CN group, hydrolyzing electronegative intermediates to then converting the six-membered ring intermediates into amides. Finally, fibers containing —COOH groups are formed after further attack of $OH^-$. (For interpretation of the references to color in this figure legend, the reader is referred to the web version of this article.)

30 mm × 1 mm, the tensile force was 5 N, and the tensile rate was 5 mm/min. To verify the tensile strength of the membranes in aqueous media, the membranes were first soaked in water for 48 h, then removed, and the excess of water on the surface was wiped off with filter paper. The pore sizes of the membrane were measured by a Microfiltration Membrane Pore Size Analyzer (PSDA-20, Nanjing Gao Qian Functional Materials Technology Co., Ltd., China) and TriStar II Plus BET Gas Adsorption Analyzer (Scientificinc). The porosity (ε) was obtained by calculating the wet and dry mass of the membrane from Eq. (1) [39]:

$$\varepsilon = \frac{(mass_{wet} - mass_{dry})/\rho_w}{area_{membrane} \times thickness_{membrane}} \times 100\% \quad (1)$$

where $\rho_w$ is the density of ethylene glycol. Typically, the membrane was completely immersed in the ethylene glycol, then the excess solvent was wiped off the membrane surface with filter paper. The water contact angle (WCA, 5 μL) and underwater oil contact angle (UOCA, 5 μL) were measured by using an OCA20 contact angle meter (Dataphysics, Bad Vilbel, Germany). The droplet diameter of the O/W emulsion (4–20 μm) was measured with an optical microscope (Olympus Corporation, Japan). The topography of the membrane was tested by Theta Flex 300-Pulsating Drop 200 Tensiometer (Biolin Scientific). The thickness change of the wet membrane was also observed using the tensiometer. Briefly, the membranes were attached to a glass slide (thickness of 1 mm) using a double-sided tape. The cross-sectional photos of the membrane before and after soaking in water were obtained and the thickness of the membrane measured from the images.

### 2.4. O/W emulsion separation

The oils used in this study included *n*-hexane, toluene, petroleum, diesel, and soybean oil. SDS was used as an emulsifier and stabilizer of the O/W emulsions. Typically, the O/W emulsions were prepared by mixing oil (2 ml), water (98 ml), and SDS (3 mg) [40]. Subsequently, the solution was emulsified with a homogenizer (10 000 rpm, 20 min, D-160, Scilogex) yielding emulsions that were stable for more than 24 h.

For O/W separation, the respective CNC/H-PAN membrane was sealed between vertical glass tubes, giving an effective membrane filtration area of 18.18 × $10^{-5}$ $m^2$. In a typical experiment, an O/W emulsion was slowly added to the upper glass tube (system height at 12–15 cm). The separation experiments were carried out under gravity. The flux (*F*) was evaluated from the permeation volume during 3 min, Eq. (2) [41]:

$$F = \frac{V}{At} \quad (2)$$

where *V* (L) is the permeation volume through the membrane; *A* ($m^2$) is the effective filtration area; *t* (h) is the filtration time. The oil content in the emulsion and filtrate was determined by total organic carbon (TOC) meter (TOC-L20 Shimadzu, Japan). The separation efficiency ($\eta$) of the sample was determined using Eq. (3):

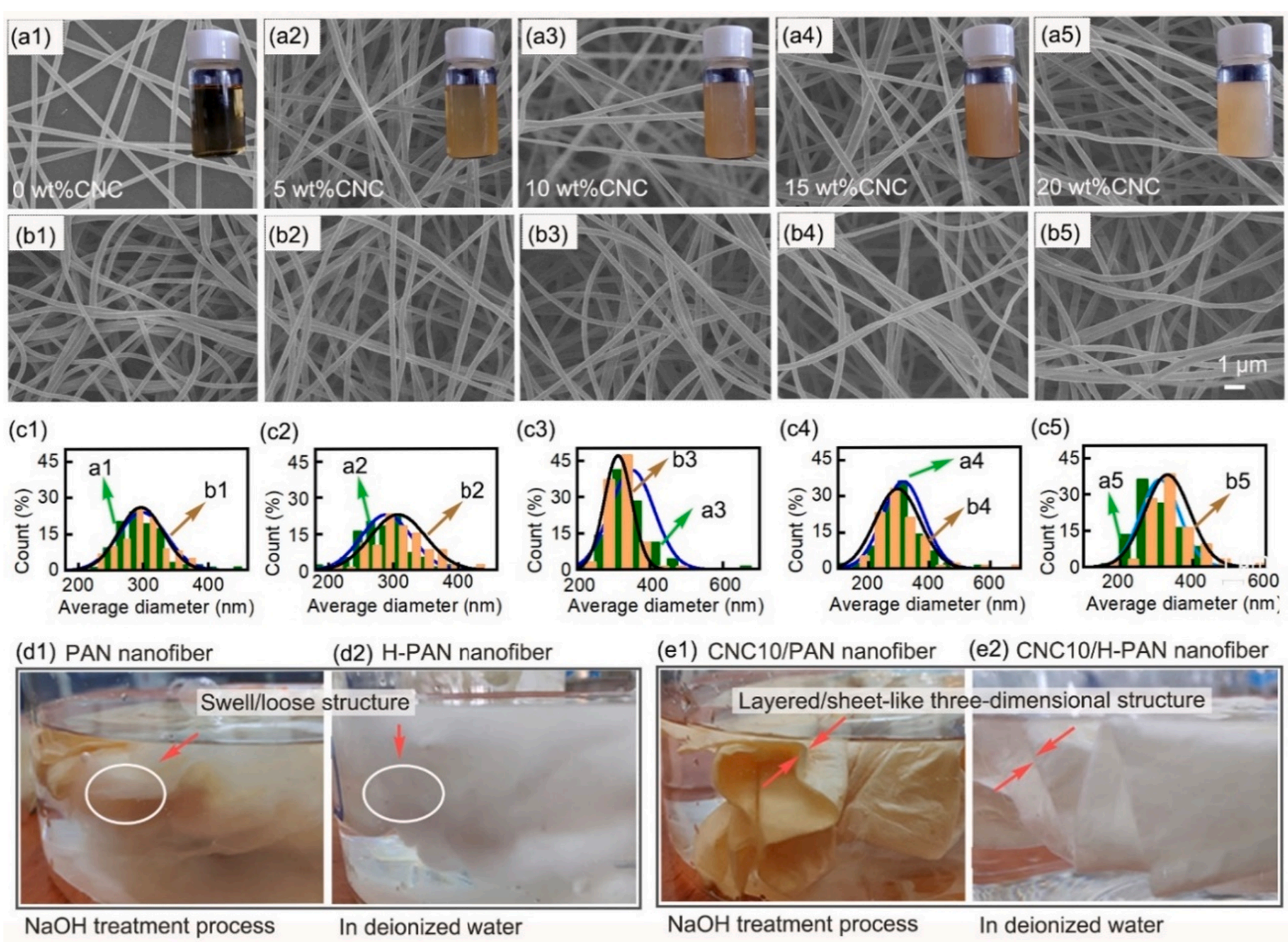


**Fig. 2.** SEM image of the (a) CNC/PAN, (b) CNC/H-PAN composite nanofibers reinforced with CNC at given concentrations, and (c) size distribution of the nanofibers. The insets correspond to the spinning solutions. (d, e) Photos of the PAN and H-PAN membranes upon hydrolysis. The circles are used to highlight the effect of the aqueous medium in membrane swelling, the color of the PAN fiber membrane changed from white to yellow, which is related to the six-membered ring intermediate in the hydrolysis process. (e) The addition of CNC in PAN and H-PAN produces less swollen, sheet-like three-dimensional membrane structures (see arrow). (For interpretation of the references to color in this figure legend, the reader is referred to the web version of this article.)

$$\eta = \frac{C_f - C_p}{C_f} \times 100\% \quad (3)$$

where $C_f$ and $C_p$ are the total organic carbon (TOC) content of the emulsion feed and filtrate.

## 3. Results and discussion

### 3.1. Nanofiber morphology

The morphology of the ENM composed (CNC-reinforced PAN nanofibers), before and after alkali hydrolysis, is shown in Fig. 2, and Figs. S1–S3. Both PAN and hydrolyzed PAN (H-PAN) nanofibers swelled in aqueous media, resulting in a loose fibrous structure (Figs. 2d, S3). As shown in Fig. 2d, the poor structural stability limits the reusability of the PAN nanofiber membrane, which is unfavorable for their application. Therefore, we introduced CNC to produce composite nanofibers, Fig. 2e. With CNC addition, the as-fabricated membrane maintained its flexibility and compliance, as can be observed during the hydrolysis process (Fig. S3). This is mainly because hydrolysis induced rearrangement of hydrogen (H)-bonding interactions between the —OH groups in CNC units and the —COOH groups in H-PAN units. A cross-linked network is formed between nanofibers, realized in the presence of CNC, which in turn enhances the three-dimensional stability of the structure. The change in the thickness of the fiber membrane upon immersion in water indicated that CNC plays an important role in enhancing the stability of the structure (Fig. S4). The addition of CNC effectively prevents membrane swelling, and the thickness of the wet membrane decreased (Fig. S5a).

Compared with the CNC/PAN composite membranes (Fig. 2a1-5), the CNC/H-PAN system (Fig. 2b1-5) maintained the original nanofiber structure of the as-spun nanofiber before hydrolysis. The average diameter changed from 296 ± 34 nm to 330 ± 61 nm with the increased CNC loading in CNC/PAN. Likewise, the difference (maximum value - minimum value) of the nanofiber diameter increased (Table S1). This observation is explained by the fact that CNC increases the viscosity of the polymer solution (Table S2) and reduces the Rayleigh instability: the lack of compatibility between the lipophilic nitrile groups (—C≡N) of PAN chains and the hydrophilic hydroxyl groups (—OH) of CNC led to jet instabilities during the spinning process, yielding a more uneven and increased fiber diameter. Besides, CNC loading also changed the conductivity and surface tension of the spinning solution (Table S2), which affect the stability of the spinning jet.

For CNC/H-PAN (Fig. 2), hydrolysis mainly occurred on the surface, as confirmed by FT-IR and XPS (Fig. S2, Supporting Information). In Fig. S2a, the absorption peak at 2242 $cm^{-1}$ was weakened, and the peak at 1668 $cm^{-1}$ disappeared. A weak absorption peak appeared at 1358 $cm^{-1}$. These changes in absorption indicate that the —CN groups in CNC/PAN were hydrolyzed. In Fig. S2b, the O element content of CNC/H-PAN was higher than that of CNC/PAN. Meanwhile, N content decreased from 17.0 % to 15.2 %. No protonation of amino groups in CNC/PAN was evident, Fig. S2c-d, while the peak intensity of (C=O) in CNC/H-PAN increased. These differences in functional groups evidenced the changes in CNC/H-PAN surface composition [37,42]. As CNC increased, the fibers displayed a smooth surface (Fig. 2b). While CNC did not change the fiber morphology, it can change the diameter and distribution of the fibers (Fig. 2c), as well as the integrity of the membrane structure (Fig. 2d–e), and water absorption capacity (Figs. S4, S5a). The CNC/H-PAN composite membranes absorbed moisture and swelled during hydrolysis due to the amphiphilicity of PAN. As shown in Fig. S5a, the water uptake capacity of the composite membrane was as high as 25 times higher compared to its mass, and the water uptake capacity decreased with CNC loading. The hydrogen-bonded cross-linked network of CNC and hydrolyzed PAN limited the water swelling of the membrane. Moreover, during the drying process, the evaporation of water led to the strengthening of CNC intermolecular hydrogen-bonding interactions within the nanofibers, resulting in nanofiber shrinkage.

### 3.2. Membrane stability

Fig. 3 and Table S3 show the mechanical properties of CNC/H-PAN composite ENMs. The competing effects of H-bonding interactions between adjacent nanofibers and CNC agglomeration contribute to tensile strength ($\sigma_{max}$) and elongation at break ($\varepsilon_b$) that increased first and then decreased with CNC loading. Meanwhile, Young's modulus ($E$) showed an increasing trend with CNC addition. For the H-PAN ENMs, there were only limited attractive interactions between adjacent nanofibers (*e.g.*, hydrogen bonds). The —$CONH_2$ and —COOH groups in H-PAN can form hydrogen bonds [43]. The strength of the as-spun nanofiber membrane was mostly dependent on the intrinsic integrity of individual nanofibers, which were more easily displaced and broke under the action of external forces. The $\sigma_{max}$, $\varepsilon_b$, and $E$ values were 1.93 MPa, 48.9 %, and 4.89 MPa (for H-PAN), respectively. Moreover, the nanofibers distribution was relatively loose and disordered, and the interaction between adjacent fibers was weak [38]. Such a loose structure was demonstrated by the relatively small bulk density of the H-PAN membrane (0.1333 $g/cm^3$, Table S4). In the initial stage of stretching, the arrangement between the nanofibers changed from loose to tight. With a further increase in stress, the composite fibrous membrane became fully stretched. Hence, single nanofibers withstood the tensile stress, and the strain increased linearly with the load, until rupture, Fig. 3f.

The addition of CNC changed the arrangement and microstructure of the nanofibers. For the CNC-5/H-PAN ENMs (Table S3), the $\sigma_{max}$, $\varepsilon_b$, and $E$ values were 3.71 MPa, 60.4 %, and 3.68 MPa, respectively. Compared with the pristine H-PAN ENMs, the respective $\sigma_{max}$, and $\varepsilon_b$ values increased by 92.2 %, and 23.6 %, respectively. Correspondingly, CNC-10/H-PAN ENMs (Fig. 3a–b), showed $\sigma_{max}$, $\varepsilon_b$, and $E$ values of 4.2 MPa, 62.83 %, and 9.8 MPa, respectively. Compared with the H-PAN ENMs, $\sigma_{max}$, $\varepsilon_b$, and $E$ values of the CNC-10/H-PAN ENMs increased by 117.6 %, 28.6 %, and 100.4 %, respectively. These improvements in ENM's tensile strength can be explained by the hydrolysis-induced rearrangement of the hydrogen bond interactions between CNC and PAN groups, which also led to an increased bulk density of the membrane (Table S4). The main groups in H-PAN fibers are —COOH, —$CONH_2$, and the unhydrolyzed —CN. These groups form hydrogen bonds, with —COOH being particularly relevant [43]. In the presence of CNC, increases the density of hydrogen bonding. During the stretching process, the H-bonding interaction prevented the adjacent nanofibers from slipping and underwent stress changes together with the surrounding nanofibers (Fig. 3b–e). Therefore, the membrane was able to sustain large external forces.

The mechanical strength of the ENMs declined when CNC was used in excess (15 % loading). This observation is related to changes in the physical and chemical properties (viscosity, conductivity, surface tension, Table S2) of the spinning precursor, all of which lead to the undesired increase of jet instability during spinning. Nanofibers with small and uneven diameters appeared due to jet splitting. As a result, the tensile strength of the composite membrane decreased. The elongation at break decreased and the toughness of the material deteriorated. As the CNC was further increased to 20 %, agglomeration took place in the spinning solution, which further affected adversely the interfacial compatibility between CNC and H-PAN. As shown in Fig. S5b, the wet CNC10/H-PAN membrane showed the higher tensile strength ($\sigma_{max}$ and $\varepsilon_b$ of 4.8 MPa and 95 %, respectively) (Fig. 3a).

In summary, CNC-10/H-PAN ENMs had a high density (bulk density) and uniform fiber diameter distribution (Fig. 2). In addition, intermolecular hydrogen bonding interactions (formed by hydroxyl groups of CNC and carboxyl groups in H-PAN) between adjacent nanofibers prevented the nanofibers from slipping.

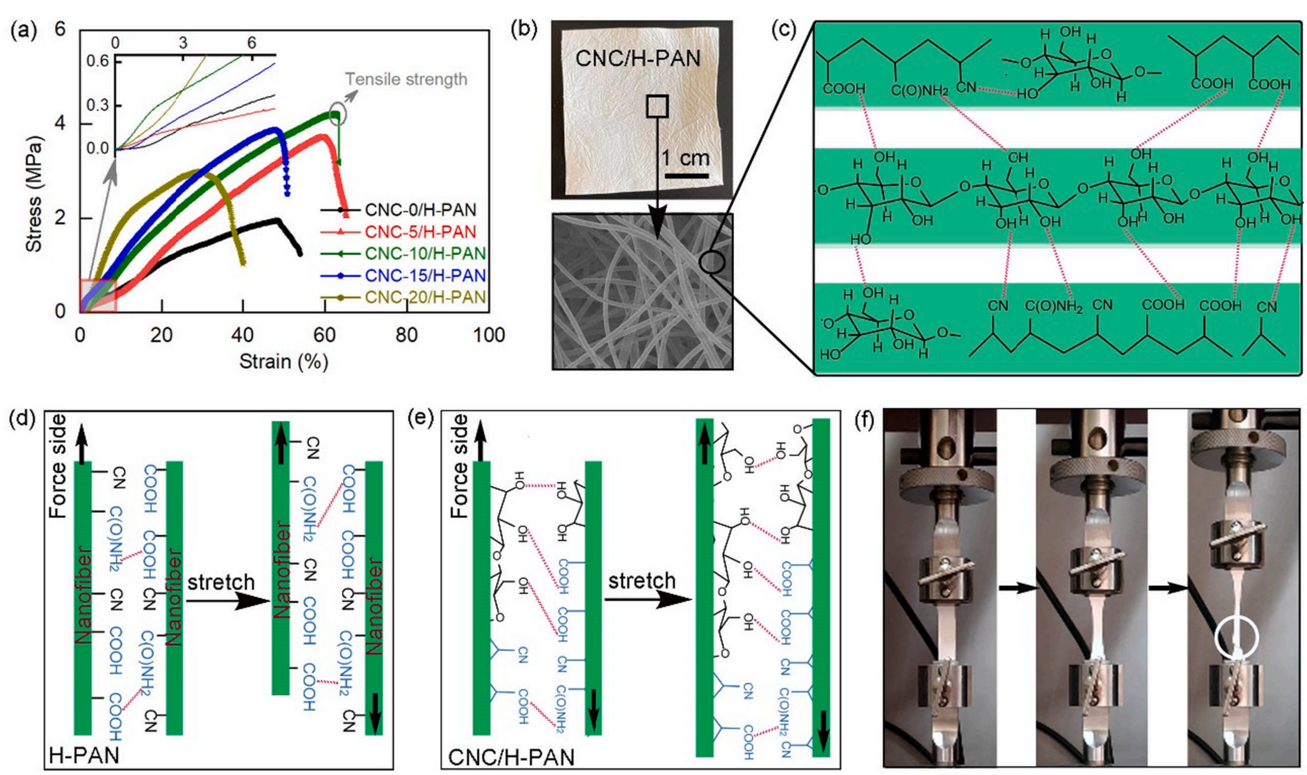

**Fig. 3.** Mechanical properties of CNC/H-PAN composite nanofiber membranes: (a) Stress–strain curve of the membranes with CNC loading; (b) Optical image of the membrane; (c) Schematic diagram of intertwined nanofibers and molecular depiction of hydrogen bonding interactions within the nanofibers; (d) nanofibers in PAN membranes separate in the process of stretching due to the lack of interaction between the adjacent nanofibers; (e) addition of CNC (CNC-10/H-PAN) imparted molecular interactions between neighboring nanofibers and enhanced the mechanical properties of the membranes; (f) A membrane subjected to tensile test until failure. (For interpretation of the references to color in this figure legend, the reader is referred to the web version of this article.)

### 3.3. Pore structure

We used the $N_2$ adsorption–desorption and bubble point methods to analyze the micro/nano hierarchical pore structure of the membrane, respectively. As shown in Fig. 4d, the $N_2$ adsorption–desorption isotherms of CNC/H-PAN membranes correspond to type II isotherms, which belong to single-layer reversible adsorption on non-porous solid surfaces [44]. The result indicated that there was no obvious secondary

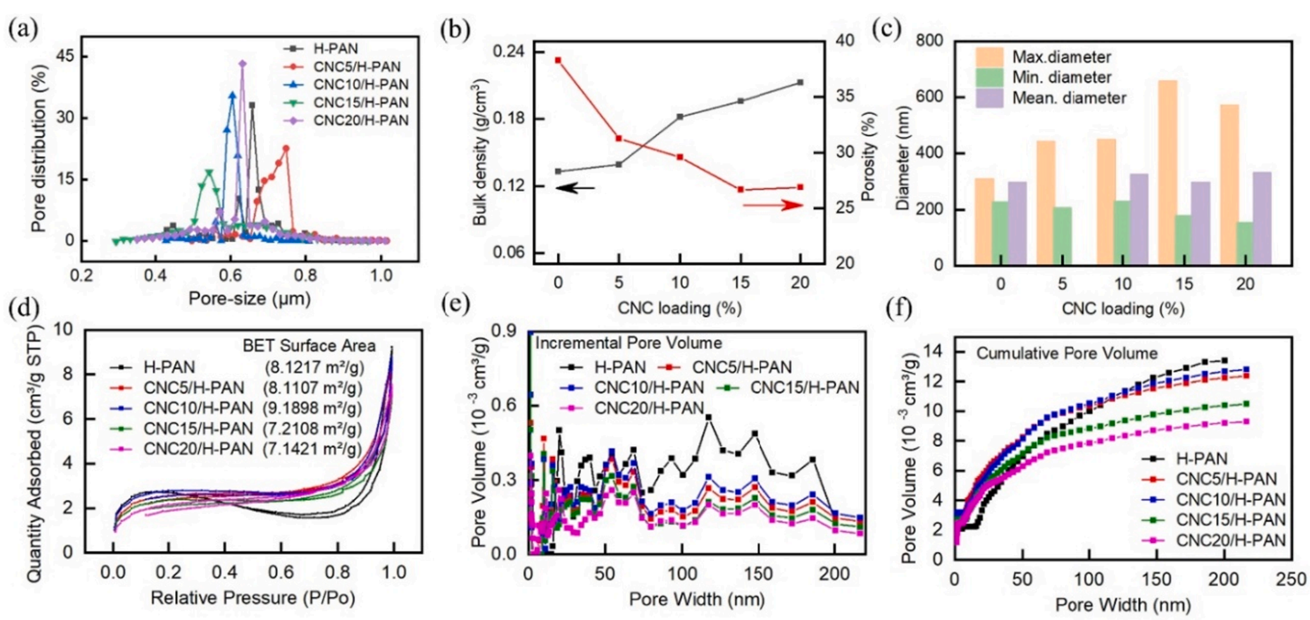

**Fig. 4.** (a) Pore size distribution (PSD) profile of CNC/H-PAN ENMs obtained by the bubble point method, and (b, c) physical properties of the nanofibers and membrane structure. (d) $N_2$ adsorption–desorption isotherm of membranes (e, f) Pore size distribution (PSD) curve calculated by DFT method according to N2 adsorption–desorption isotherm. (For interpretation of the references to color in this figure legend, the reader is referred to the web version of this article.)

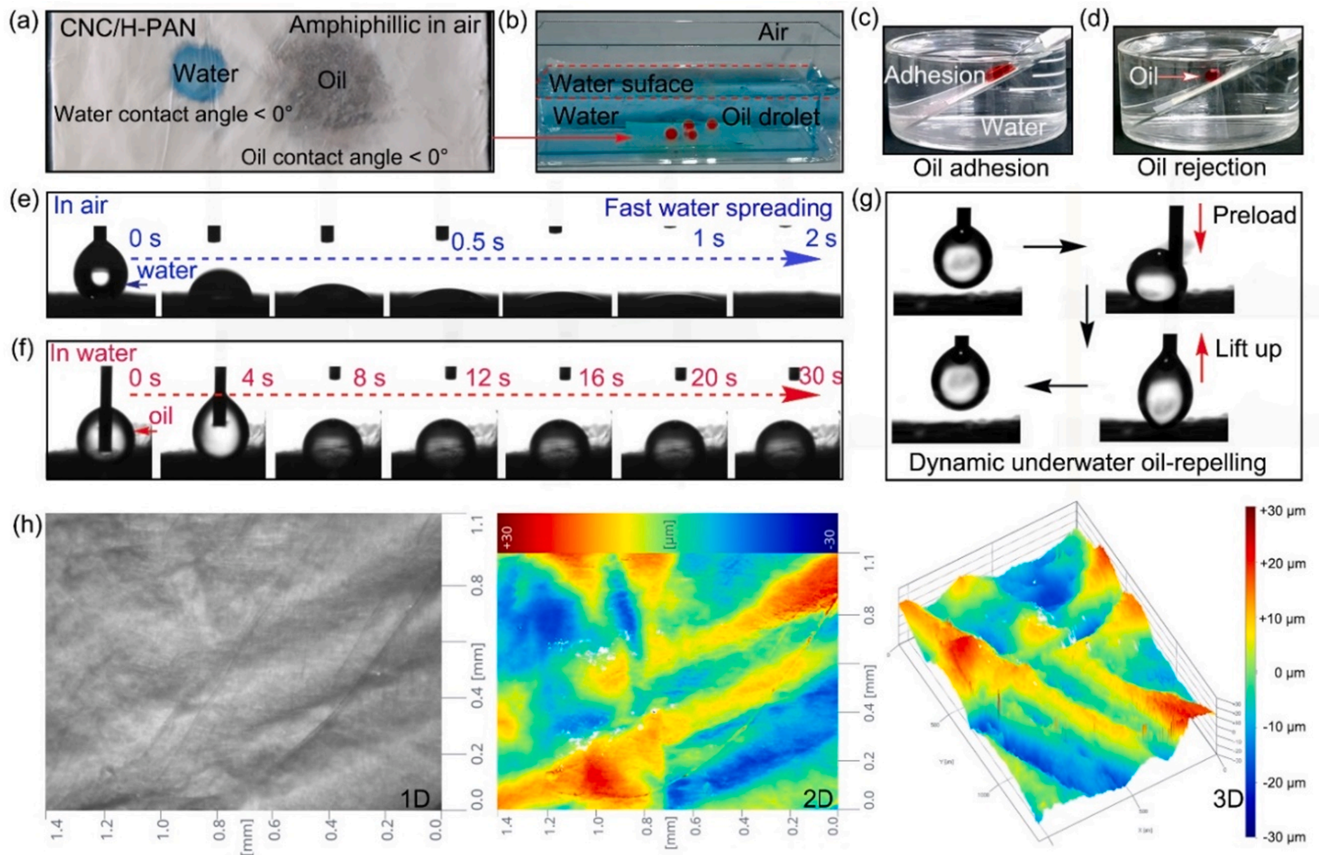


**Fig. 5.** The CNC-10/H-PAN ENM: (a) The amphiphilicity of the ENM to water and oil. (b) Photographs of underwater super-oleophobic effect. (c–d) The underwater oil dynamic adhesion for CNC/PAN and CNC/H-PAN ENM. (e) Dynamic water (5 μL) contact angle was measured on the surface of the membranes. (f) Dynamic underwater oil (10 μL) contact angle of the membrane. (g) Images displaying underwater oil repellency (5 μL). Note: the oil was 1,2-dichloroethane (dyed with oil red), and water was dyed with methylene blue. (h) 1D, 2D, 3D topography of CNC-HPAN membrane (Horizontal Ra = 3.9 μm, Vertical Ra = 0.59 μm). (For interpretation of the references to color in this figure legend, the reader is referred to the web version of this article.)

structure formation on the surface of single nanofibers in the membrane, which is consistent with the SEM results in Fig. 2b. The pore size distribution (PSD) of the nanofiber membrane was quantitatively analyzed based on density functional theory (DFT). The PSD curve of the CNC/H-PAN membrane did not show any distribution peaks (Fig. 4e), indicating the absence of a nanoscale pore structure. With the addition of CNC, the specific surface area of the membranes was slightly decreased (from 8.12 $m^2$ $g^{-1}$ to 7.14 $m^2$ $g^{-1}$). The decrease in cumulative pore volume further indicated that the CNC had an important effect on the formation of smooth surfaces on individual nanofibers (Fig. 4f).

Fig. 4a presents the ENMs, which display a pore size distribution centered around 0.5–0.8 μm. For H-PAN/CNC-0, -5, -10, -15 and -20, the average pore sizes were 0.65, 0.74, 0.60, 0.54, and 0.63 μm, respectively. The average pore size of the membranes increased with CNC loading, up to a maximum. This observation is attributed to the increased fiber diameter and the wider range of diameter distribution (Fig. 4c and Table S4). As shown in Fig. 4b–c, both the fiber diameter and bulk density showed an increasing trend with CNC content. The increase of bulk density directly leads to reduced porosity. The increasing fiber diameter leads to large porous ENM structures. The hydrogen bonding with CNC increases the bulk density of the membrane, as discussed earlier in the context of the SEM images, Fig. 2. In the absence of CNC (*i.e.*, H-PAN ENM), the interactions between nanofibers were weak. Therefore, the nanofiber or nanofiber layers were easy to peel off after absorbing water, *e.g.,* during hydrolysis. In such conditions, the membranes swell (supporting information Fig. S3). For CNC-5/H-PAN, hydrogen bonding was relatively weak, and ENM pore structure was mainly affected by the nanofiber diameter. Therefore, CNC5/H-PAN had the largest average pore size and wider pore size distribution (PSD) (Fig. 4). When the CNC content further increased, the pore structure of the membrane was mainly affected by hydrogen bonding with CNC; thus, the fiber density increased, and the pore size and the PSD range of the ENMs became smaller.

When the CNC content exceeded 15 %, the number of CNC particles present on the nanofiber surface was limited, and excess CNC particles in PAN-based nanofiber underwent agglomeration, which led to the weakening of hydrogen bonding interaction that exists between CNC (—OH) and H-PAN (—COOH). The CNC20/H-PAN and CNC15/H-PAN had similar diameter distribution and porosity (Figs. 2c and 4b), but CNC20/H-PAN had a larger average fiber diameter, which was the main reason for the increased pore size between nanofibers compared to the CNC15/H-PAN (Fig. 4a). Therefore, in this study, the diameter distribution of nanofibers and the hydrogen bonding interaction between fibers became the main factors for the variation of fiber membrane pore size, which can be adjusted by introducing a certain amount of CNC in the composite membrane. Also, membranes with given CNC loading showed an enhanced interaction between fibers, improving the durability of the membrane.

### 3.4. Wettability

The wettability of materials mainly depends on surface microstructure and chemical functional groups [45], which can be adjusted by hydrolysis. Partial hydrolysis imparted hydrophilicity and underwater oleophobicity to the membrane without damaging the nanofiber structure. Meantime, the hydroxyl groups of CNC form a stable hydrogen bond cross-linking network with the carboxyl groups of the hydrolyzed PAN. Given that the interactions between nanofibers were strengthened, the composite membrane was endowed with a stable, strong three-dimensional structure (Fig. 2e). As shown in Fig. 5a, the CNC/H-PAN membrane exhibited amphiphilic properties for water and oil, given the presence of hydrophilic amide groups and polar nitrile groups [44]. Hence, the droplets (either water or oil droplets) spread quickly on the surface of the ENMs (Fig. 5). Furthermore, the interpenetrated (Fig. 2 SEM), highly porous (Table S4) membranes accelerated the penetration rate of droplets. Fig. 5b, and 5f show the underwater oleophobic effect of the CNC/H-PAN membrane. When the container (Fig. 5b) was gently shaken, oil droplets on the surface of the membrane were clearly observed (Video S1). Water penetrated the composite membrane and formed a “hydrated layer” on its surface, which had a repelling effect for oil, and could effectively prevent ENM fouling. Therefore, the underwater oil rolling was enhanced. 3D topography of the CNC/H-PAN membrane displayed a relatively rough surface (Fig. 5h), which contributed to the Cassie state and produced underwater oleophobicity [46].

To further verify the hydrophilicity and underwater oleophobicity of the CNC/H-PAN ENMs, the dynamic contact angles of the membranes were measured (Video S2–S3). As shown in Fig. 5e, water rapidly penetrated the ENMs (Video S2). Fig. 5f shows that the ENMs presented underwater oleophobicity (the oil droplets could remain relatively stable for a long time when immersed in aqueous media, Video S3). However, the oil resistance of the ENMs directly affected the membrane filtration efficiency and surface chemical modification enhanced the resistance to oil. Fig. 5c–d corresponds to the underwater oil rolling test before and after the hydrolysis of the ENMs. The CNC/PAN composite membrane displayed underwater oleophobicity, but poor oil resistance (Fig. 5c and Video S4). When in contact with the ENMs, oil droplets adhered to the surface of the ENMs. Then oil droplets began to merge and eventually settled. This fouling behavior caused the membrane’s surface to become covered with oil droplets and deteriorated its selective wettability [47]. Upon membrane hydrolysis (CNC/H-PAN), the oil resistance and underwater oleophobicity were significantly improved, and the oil droplets could quickly slide (Video S4). This was mainly because the hydrolysis converted some of the nitrile and amide groups on the membrane into carboxyl groups. A dynamic underwater oil-repelling experiment was conducted (Fig. 5g), evidencing a remarkable underwater oil-repelling effect.

### 3.5. Emulsion filtration

The sliding of fibers during emulsion separation lead to an enlargement of the void spaces between the fibers. Moreover, with surface fouling, the transmembrane pressure increases, and the fiber sliding becomes easier, which in turn leads to an easier penetration of oil droplets [30]. CNC has a reinforcement effect *via* hydrogen-bonding, which further increases the structural stability of the membrane and prevents fiber slippage. The excellent anti-fouling performance of the H-PAN membrane made it most suitable for emulsion separation. Fig. 6 shows a CNC-10/H-PAN membrane and provides a schematic illustration of the O/W emulsions separation process. The oil phase was dyed with Sudan III to facilitate the observation of the separation process (Supporting information, Fig. S6, and Video S5 for hexane/water emulsion). The two-phase fluid was turbid before filtration and the polarized microscope image (Fig. 6b) confirmed the emulsion type as being oil-in-water (O/W). This observation means that O/W emulsions can be easily separated by gravity on the CNC-10/H-PAN membrane (Fig. 6a). After filtration, a uniform, transparent solution was obtained (with no free droplets observed, Fig. S6), indicating that the oil and water phases were effectively separated.

During the filtration process, the ENM was covered with a hydration layer and small oil droplets were trapped on the surface, then flocculated (Fig. S6). As the water droplets continued to penetrate, liquid transport continuously occurred on the surface of the membrane (Figs. 7, S6, and Video S5), thereby accelerating free collisions and fusion of the oil droplets on the surface of the membrane. When the oil droplets (2–30 μm, Fig. S7) increased to a certain size (buoyancy > gravity), the oil droplets started to float and were spontaneously removed from the membrane surface (Video S5). The formed “hydration” layer was mainly related to the affinity properties of PAN-based nanofibers [39]. The addition of CNC and the modification of PAN endowed the ENMs with higher hydrophilicity. It was demonstrated that the dense H-bonding network in the CNC/H-PAN membrane not only enhanced the mechanical robustness and shape retention but facilitated the separation of the O/W emulsions (Fig. 7a, f). By contrast, the CNC-free, H-PAN membrane (Fig. 7g, h) is ineffective. The presence of the “hydration layer” hindered the contact of oil droplets with the membrane surface. Thereby, the underwater oleophobicity of the ENMs and the oil rolling effect for the ENMs were both enhanced (Fig. 5f and Video S4).

Fig. 7 shows the separation flux, efficiency, and cycle stability of an

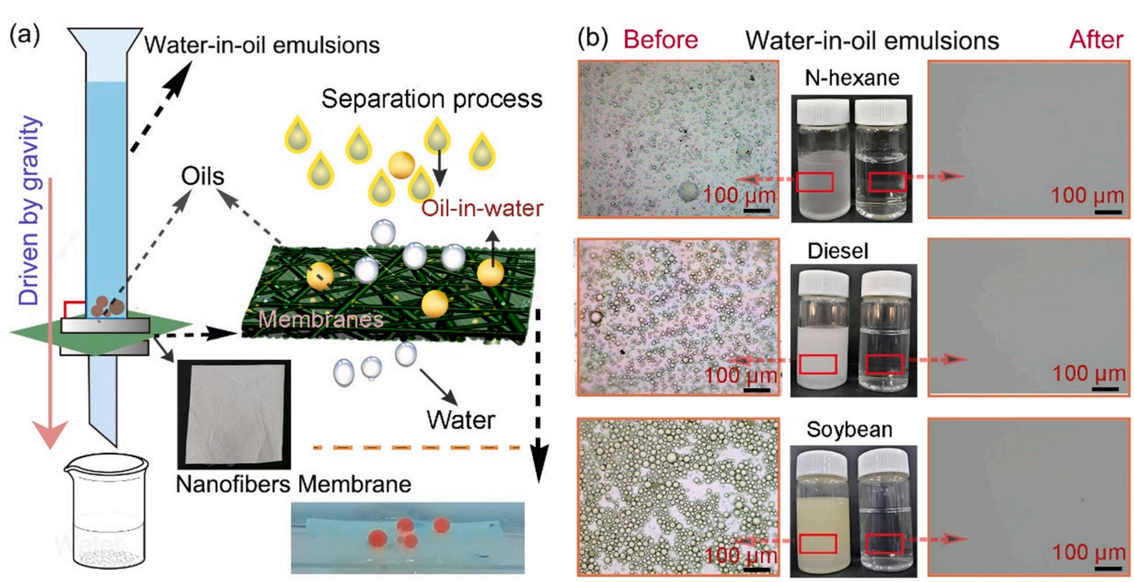


**Fig. 6.** (a) Schematic diagram of O/W emulsions separation process (b) Optical microscope image of O/W emulsion before (left) and after filtration (right for the filtrate). (For interpretation of the references to color in this figure legend, the reader is referred to the web version of this article.)

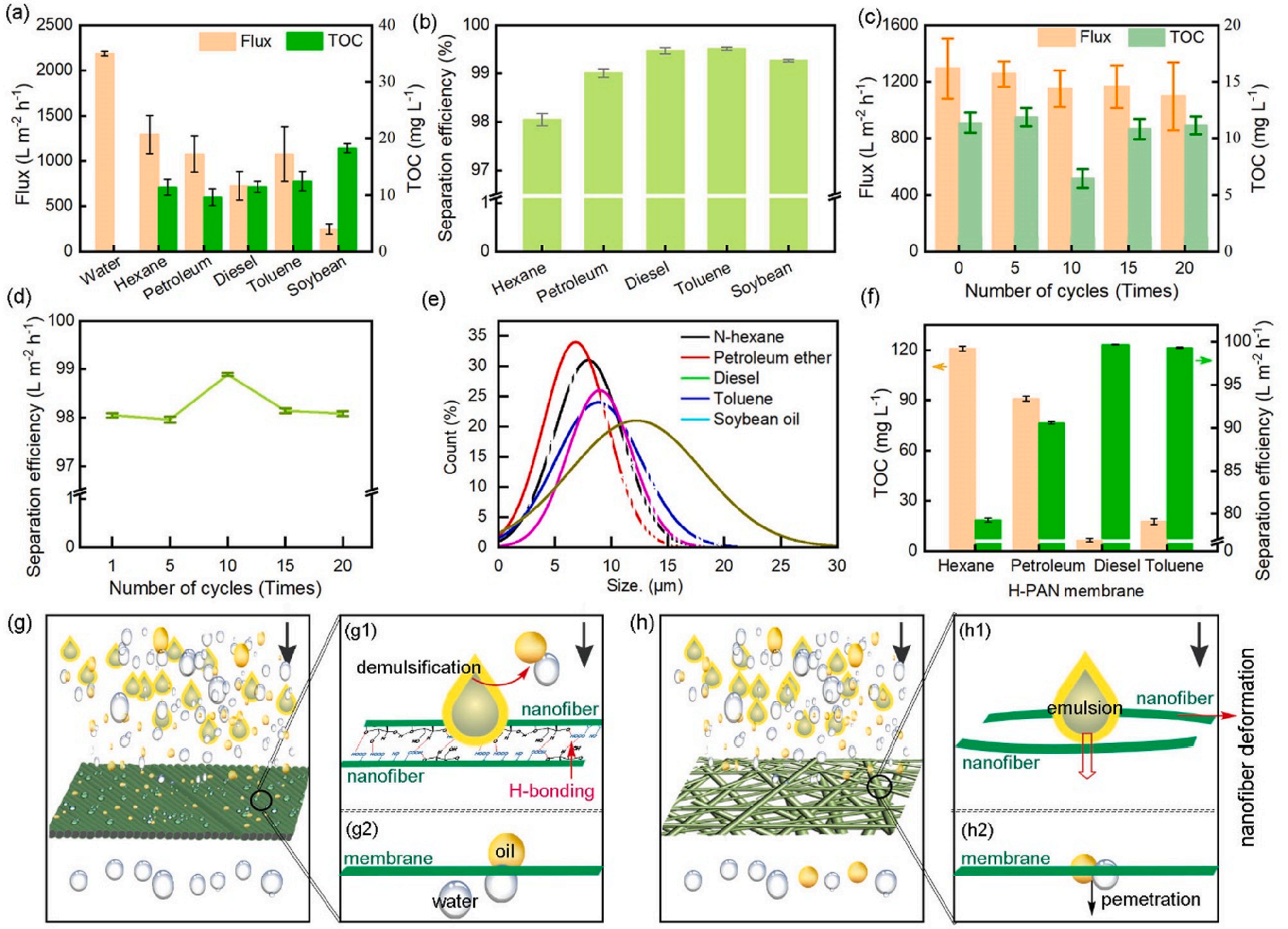

**Fig. 7.** CNC/H-PAN ENMs used to filter O/W emulsions: (a) Flux, TOC value, and (b) separation efficiency; (c) Flux, TOC value, and (d) separation efficiency of hexane-in-water emulsion processes with the CNC/H-PAN membrane for 20 cycles; (e) Size distribution of O/W emulsions measured in optical microscope image images. (f) TOC value and separation efficiency of H-PAN ENMs used to filter O/W emulsions. (g) The dense H-bonding network in the membrane is responsible for its mechanical robustness and contributes to shape retention and enhanced O/W emulsion separation. (h) IN the absence of the hydrogen bond network, the membranes deformed during emulsion separation and failed to maintain a stable pore structure. (For interpretation of the references to color in this figure legend, the reader is referred to the web version of this article.)

O/W emulsion processed with the CNC-10/H-PAN membrane (with high mechanical strength, as discussed in Section 3.2). The TOC values of the filtrate before separation are included in Table S5. After the first separation (all O/W emulsions), the TOC value measured in the filtrate was < 15 mg/L. Especially for the hexane-in-water emulsion, the TOC content after filtration was < 12 mg/L, and the separation efficiency reached 98 %. The separation fluxes of the ENMs for *n*-hexane, petroleum ether, diesel, toluene, and soybean oils were 1293, 1078, 724, 1076, and 245 $L{\cdot}m^{-2}h^{-1}$, respectively. The corresponding separation efficiencies were 98.2, 99.1, 99.5, 99.5, and 99.3 %. Meanwhile, the water flux was as high as 2186 $L{\cdot}m^{-2}h^{-1}$.

Fig. 7c-d shows the separation flux and filtration efficiency of the CNC/H-PAN membrane for hexane-in-water emulsion following 20 cycles. The flux decreased gradually with the number of cycles but the efficiency remained largely unchanged. The main reason for this observation is that the hydrophilic CNC/H-PAN swells in the presence of water and forms a gel-like layer on the surface of the composite membrane (Fig. S3-c2 and Fig. S8a). Impurities such as dye in the solution are deposited on the surface of the gel layer (Fig. S8b), and the flux of the membrane decreases. When the ENMs were rinsed with deionized water (Fig. S8c), the flux was completely recovered (Fig. 7c). Notably, after 20 testing cycles, the flux and efficiency of ENMs were still over 1096 $L{\cdot}m^{-2}h^{-1}$ and 98.2 %.

The membranes have an interpenetrating nanofiber pore structure (Fig. 2, SEM). After fiber swelling, surface hydration effectively prevented the impurities (dye) from diffusing into the material [44]. The presence of CNC improved the mechanical strength of the ENMs (Fig. 3) by introducing the hydrogen bonding network. Nanofibers in the CNC-free H-PAN membrane were easily deformed during the separation of emulsion and failed to maintain a stable pore structure (Fig. 7h), resulting in poor separation efficiency (Fig. 7f). The non-hydrolyzed PAN membrane was ineffective for the separation of emulsions due to oil fouling (Fig. 5c). Thus, the introduction of CNC and hydrolyzed PAN are critical to ensure the durability of the membrane. Fig. S9 corresponds to the SEM and normal distribution of the composite nanofiber membrane obtained after 20 filtration cycles. Compared with the original composite membrane, no significant change in microstructure was noted.

## 4. Conclusion

Hydrolyzed polyacrylonitrile was loaded with cellulose nanocrystals (CNC/H-PAN) as the precursor of electrospun nanofibrous membranes (ENM) that were tested for the separation of multiphase systems. The dispersed reinforcing phase, CNC, contributed to superior three-dimensional structural stability and durability. PAN hydrolysis induced the formation of hydrogen (H)-bonding between CNC and H-PAN. The dense H-bonding network in the CNC/H-PAN membrane was responsible for the mechanical robustness, contributing to shape retention, and enhancing the emulsion separation performance (oil-in-water, O/W). CNC-free H-PAN membranes showed an apparent loss of structural integrity, for instance, when immersed in aqueous media. The individual nanofibers in the H-PAN membranes were prone to displacement and rupture under the action of external forces. This effect is a result of the lack of H-bonding interactions between adjacent nanofibers. The addition of CNC enhanced molecular interactions between neighboring nanofibers. The CNC-10/H-PAN membrane displayed high stability: tensile strength of 4.2 MPa and elongation at break of 62.83 % (117.6 % and 28.6 %, respectively, higher than the corresponding values for unfilled H-PAN ENM).

The membranes exhibited water and underwater oil contact angles of 0° and 141°, respectively. Such differences in membrane wettability contributed to antifouling and oil adhesion resistance. The combination of pore size and antifouling effects led to ENMs with high water flux (2186 $L\cdot m^{-2}\cdot h^{-1}$) and were shown to be effective in emulsion separation under gravity gradient. The membranes further showed excellent separation ability and recyclability.

Hexane-in-water emulsions indicated membrane flux and filtration efficiency of 1293 $L\cdot m^{-2}\cdot h^{-1}$ and 98.2 %, respectively. After 20 filtration cycles, the microstructure of the membranes remained relatively stable, with an emulsion flux of 1097 $L\cdot m^{-2}\cdot h^{-1}$, and a separation efficiency that was kept largely unchanged (98.2 %). By contrast, the CNC-free H-PAN membrane failed to maintain a stable pore structure, resulting in poor separation performance. Moreover, the non-hydrolyzed PAN underwent oil fouling, preventing emulsion separation. Therefore, the introduction of CNC and the hydrolysis of PAN are necessary steps to ensure the durability of the ENMs. Overall, the introduced membranes have excellent structural stability, durability, and resistance during filtration, and offer excellent prospects in the field of multiphase separation.

## Declaration of Competing Interest

The authors declare that they have no known competing financial interests or personal relationships that could have appeared to influence the work reported in this paper.

## Data availability

No data was used for the research described in the article.

## Acknowledgment

This work was financially supported by the Natural Science Foundation of Heilongjiang Province (Grant No. LH2020C039), the Fundamental Research Funds for the Central Universities (Grant No. 2572019AB02), H2020-ERC-2017-Advanced Grant 'BioELCell' (788489), the Canada Excellence Research Chair Program (CERC-2018-00006) and the Canada Foundation for Innovation (Project number 38623).

## Appendix A. Supplementary material

Supplementary data to this article can be found online at https://doi.org/10.1016/j.compositesa.2022.107300.

## References

[1] Yin H, Zhao J, Li Y, Liao Y, Huang L, Zhang H, et al. Electrospun SiNPs/ZnNPs-$SiO_2$/$TiO_2$ nanofiber membrane with asymmetric wetting: ultra-efficient separation of oil-in-water and water-in-oil emulsions in multiple extreme environments. Sep Purif Technol 2021;255.

[2] Cao M, Xiao F, Yang Z, Chen Y, Lin L. Construction of polytetrafluoroethylene nanofiber membrane via continuous electrospinning/electrospraying strategy for oil-water separation and demulsification. Sep Purif Technol 2022;287.

[3] Zhang J, Liu L, Si Y, Yu J, Ding B. Electrospun nanofibrous membranes: an effective arsenal for the purification of emulsified oily wastewater. Adv Funct Mater 2020;30(25).

[4] Ma W, Zhang M, Liu Z, Huang C, Fu G. Nature-inspired creation of a robust free-standing electrospun nanofibrous membrane for efficient oil-water separation. Environ Sci Nano 2018;5(12):2909–20.

[5] Song C, Rutledge GC. Electrospun liquid-infused membranes for emulsified oil/water separation. Langmuir 2022;38(7):2301–13.

[6] Kahraman HT, Yar A, Avcı A, Pehlivan E. Preparation of nanoclay incorporated PAN fibers by electrospinning technique and its application for oil and organic solvent absorption. Sep Sci Technol 2017;53(2):303–11.

[7] Gong H, Li W, Zhang X, Peng Y, Yu B, Mou Y. Effects of droplet dynamic characteristics on the separation performance of a demulsification and dewatering device coupling electric and centrifugal fields. Sep Purif Technol 2021;257.

[8] Khan JA, Al-Kayiem HH, Aleem W, Saad AB. Influence of alkali-surfactant-polymer flooding on the coalescence and sedimentation of oil/water emulsion in gravity separation. J Petrol Sci Eng 2019;173:640–9.

[9] Dai J, Chang Z, Xie A, Zhang R, Tian S, Ge W, et al. One-step assembly of Fe(III)-CMC chelate hydrogel onto nanoneedle-like CuO@Cu membrane with superhydrophilicity for oil-water separation. Appl Surf Sci 2018;440:560–9.

[10] Zhu Z, Wang W, Qi D, Luo Y, Liu Y, Xu Y, et al. Calcinable polymer membrane with revivability for efficient oily-water remediation. Adv Mater 2018;30(30):e1801870.

[11] Yang HC, Pi JK, Liao KJ, Huang H, Wu QY, Huang XJ, et al. Silica-decorated polypropylene microfiltration membranes with a mussel-inspired intermediate layer for oil-in-water emulsion separation. ACS Appl Mater Interfaces 2014;6(15):12566–72.

[12] Wang B, Liang W, Guo Z, Liu W. Biomimetic super-lyophobic and super-lyophilic materials applied for oil/water separation: a new strategy beyond nature. Chem Soc Rev 2015;44(1):336–61.

[13] Lu J, Cao M, He X, Hu Y, Bai L, Huan S, et al. Electrospun hierarchically channeled polyacrylonitrile nanofibrous membrane for wastewater recovery. J Cleaner Prod 2022;361.

[14] Lu W, Duan C, Zhang Y, Gao K, Dai L, Shen M, et al. Cellulose-based electrospun nanofiber membrane with core-sheath structure and robust photocatalytic activity for simultaneous and efficient oil emulsions separation, dye degradation and Cr(VI) reduction. Carbohydr Polym 2021;258:117676.

[15] Wang Z, Crandall C, Prautzsch VL, Sahadevan R, Menkhaus TJ, Fong H. Electrospun regenerated cellulose nanofiber membranes surface-grafted with water-insoluble poly(HEMA) or water-soluble poly(AAS) chains via the ATRP method for ultrafiltration of water. ACS Appl Mater Interfaces 2017;9(4):4272–8.

[16] Zhang Z, Gan Z, Bao R, Ke K, Liu Z, Yang M, et al. Green and robust superhydrophilic electrospun stereocomplex polylactide membranes: multifunctional oil/water separation and self-cleaning. J Membr Sci 2020;593.

[17] Zhang W, Liu N, Cao Y, Lin X, Liu Y, Feng L. Superwetting porous materials for wastewater treatment: from immiscible oil/water mixture to emulsion separation. Adv Mater Interfaces 2017;4(10).

[18] Liao Y, Loh C, Tian M, Wang R, Fane AG. Progress in electrospun polymeric nanofibrous membranes for water treatment: fabrication, modification and applications. Prog Polym Sci 2018;77:69–94.

[19] Xue J, Xie J, Liu W, Xia Y. Electrospun nanofibers: new concepts, materials, and applications. Acc Chem Res 2017;50(8):1976–87.

[20] Zhang J, Xue Q, Pan X, Jin Y, Lu W, Ding D, et al. Graphene oxide/polyacrylonitrile fiber hierarchical-structured membrane for ultra-fast microfiltration of oil-water emulsion. Chem Eng J 2017;307:643–9.

[21] Zhao H, He Y, Wang Z, Zhao Y, Sun L. Mussel-inspired fabrication of PDA@PAN electrospun nanofibrous membrane for oil-in-water emulsion separation. Nanomaterials (Basel) 2021;11(12).

[22] Guo H, Chen Y, Li Y, Zhou W, Xu W, Pang L, et al. Electrospun fibrous materials and their applications for electromagnetic interference shielding: a review. Compos Part A: Appl Sci Manuf 2021;143.

[23] Cheng X, Ye Y, Li Z, Chen X, Bai Q, Wang K, et al. Constructing environmental-friendly "Oil-Diode" Janus membrane for oil/water separation. ACS Nano 2022;16(3):4684–92.

[24] Hou L, Wang N, Wu J, Cui Z, Jiang L, Zhao Y. Bioinspired superwettability electrospun micro/nanofibers and their applications. Adv Funct Mater 2018;28(49).

[25] Su Y, Fan T, Cui W, Li Y, Ramakrishna S, Long Y. Advanced electrospun nanofibrous materials for efficient oil/water separation. Adv Fiber Mater 2022.

[26] Zhu Y, Wang D, Jiang L, Jin J. Recent progress in developing advanced membranes for emulsified oil/water separation. NPG Asia Mater 2014;6(5). e101-e.

[27] Wu J, Ding Y, Wang J, Li T, Lin H, Wang J, et al. Facile fabrication of nanofiber-and micro/nanosphere-coordinated PVDF membrane with ultrahigh permeability of viscous water-in-oil emulsions. J Mater Chem A 2018;6(16):7014–20.

[28] Yue X, Li Z, Zhang T, Yang D, Qiu F. Design and fabrication of superwetting fiber-based membranes for oil/water separation applications. Chem Eng J 2019;364:292–309.

[29] Hu Y, Lü Z, Wei C, Yu S, Liu M, Gao C. Separation and antifouling properties of hydrolyzed PAN hybrid membranes prepared via in-situ sol-gel SiO2 nanoparticles growth. J Membr Sci 2018;545:250–8.

[30] Zhang L, He Y, Luo P, Ma L, Fan Y, Zhang S, et al. A heterostructured PPy/ZnO layer assembled on a PAN nanofibrous membrane with robust visible-light-induced

self-cleaning properties for highly efficient water purification with fast separation flux. J Mater Chem A 2020;8(8):4483–93.
[31] Ma H, Yoon K, Rong L, Mao Y, Mo Z, Fang D, et al. High-flux thin-film nanofibrous composite ultrafiltration membranes containing cellulose barrier layer. J Mater Chem 2010;20(22).
[32] Wang Q, Wang D, Cheng W, Huang J, Cao M, Niu Z, et al. Spider-web-inspired membrane reinforced with sulfhydryl-functionalized cellulose nanocrystals for oil/water separation. Carbohydr Polym 2022;282.
[33] Song L, Guo Y, Fan J, Fan X, Xie Y, Xiao Z, et al. Alkyl thiol grafted silver nanoparticle–decorated cellulose nanocrystals on poly(lactic acid) composites for enhanced antibacterial activity and toughening effects. Compos Part A: Appl Sci Manuf. 2022;163.
[34] Ge J, Zong D, Jin Q, Yu J, Ding B. Biomimetic and superwettable nanofibrous skins for highly efficient separation of oil-in-water emulsions. Adv Funct Mater 2018;28(10).
[35] Wang N, Zhai Y, Yang Y, Yang X, Zhu Z. Electrostatic assembly of superwetting porous nanofibrous membrane toward oil-in-water microemulsion separation. Chem Eng J 2018;354:463–72.
[36] Cseri L, Topuz F, Abdulhamid MA, Alammar A, Budd PM, Szekely G. Electrospun adsorptive nanofibrous membranes from ion exchange polymers to snare textile dyes from wastewater. Adv Mater Technol 2021;6(10).
[37] Zhang J, Pan X, Xue Q, He D, Zhu L, Guo Q. Antifouling hydrolyzed polyacrylonitrile/graphene oxide membrane with spindle-knotted structure for highly effective separation of oil-water emulsion. J Membr Sci 2017;532:38–46.
[38] Wang D, Cheng W, Wang Q, Zang J, Zhang Y, Han G. Preparation of electrospun chitosan/poly(ethylene oxide) composite nanofibers reinforced with cellulose nanocrystals: structure, morphology, and mechanical behavior. Compos Sci Technol 2019;182.
[39] Wang X, Cheng W, Wang D, Ni X, Han G. Electrospun polyvinylidene fluoride-based fibrous nanocomposite membranes reinforced by cellulose nanocrystals for efficient separation of water-in-oil emulsions. J Membr Sci 2019;575:71–9.
[40] Wang J, La H, Yan K, Zhang L, Yu QJ. Polydopamine nanocluster decorated electrospun nanofibrous membrane for separation of oil/water emulsions. J Membr Sci 2018;547:156–62.
[41] Ma W, Guo Z, Zhao J, Yu Q, Wang F, Han J, et al. Polyimide/cellulose acetate core/shell electrospun fibrous membranes for oil-water separation. Sep Purif Technol 2017;177:71–85.
[42] Deng S, Bai R, Chen JP. Behaviors and mechanisms of copper adsorption on hydrolyzed polyacrylonitrile fibers. J Colloid Interface Sci 2003;260(2):265–72.
[43] Lai C, Chao W, Hung W, An Q, De Guzman M, Hu C, et al. Physicochemical effects of hydrolyzed asymmetric polyacrylonitrile membrane microstructure on dehydrating butanol. J Membr Sci 2015;490:275–81.
[44] Ge J, Zhang J, Wang F, Li Z, Yu J, Ding B. Superhydrophilic and underwater superoleophobic nanofibrous membrane with hierarchical structured skin for effective oil-in-water emulsion separation. J Mater Chem A 2017;5(2):497–502.
[45] Zhu H, Guo Z. Understanding the separations of oil/water mixtures from immiscible to emulsions on super-wettable surfaces. J Bionic Eng 2016;13(1):1–29.
[46] Su B, Tian Y, Jiang L. Bioinspired interfaces with superwettability: from materials to chemistry. J Am Chem Soc 2016;138(6):1727–48.
[47] Tummons EN, Tarabara VV, Chew Jia W, Fane AG. Behavior of oil droplets at the membrane surface during crossflow microfiltration of oil-water emulsions. J Membr Sci 2016;500:211–24.